

AN INTERPRETIVE BALLISTIC MODEL FOR QUASI-SYMMETRIC BIPOLAR JET SYSTEMS

A. C. Raga,¹ A. Noriega-Crespo,² J. C. Rodríguez-Ramírez,¹ V. Lora,³ K. R. Stapelfeldt,⁴ and S. J. Carey²

Received 2011 April 10; accepted 2011 June 6

RESUMEN

Presentamos un modelo analítico, balístico para sistemas de chorros/contrachorros cuasi-simétricos, considerando tanto el caso no relativista como el relativista. El modelo considera la presencia de asimetrías en el tiempo y en la velocidad de eyección, las cuales producen diferencias entre las posiciones de los nudos a lo largo del chorro y del contra-chorro. Un ajuste de las predicciones del modelo no relativista a observaciones de dos flujos HH cuasi-simétricos (HH 34 y HH 111) nos permite obtener las magnitudes de las asimetrías de tiempo y velocidad de eyección de estos sistemas.

ABSTRACT

We present an analytic, ballistic model for quasi-symmetric jet/counterjet systems, considering both the non-relativistic and the relativistic cases. The model considers the presence of ejection time and velocity asymmetries, which produce offsets between the positions of the knots in jet/counterjet pairs. A fit of the non-relativistic model predictions to observations of two quasi-symmetric HH outflows (HH 34 and HH 111) allows us to obtain the magnitudes of the ejection time and velocity asymmetries of these systems.

Key Words: Herbig-Haro objects — infrared: ISM — ISM: individual objects (HH 34, HH 111) — ISM: jets and outflows — stars: formation

1. INTRODUCTION

Many HH outflows do not have well defined symmetries between the red- and blue-shifted lobes. Examples of this are HH 32 (in which the red-shifted lobe is not well developed, see e.g., Curiel et al. 1997) and HH 262 (the outflow from the L1551 IRS5 source, which shows a very complex structure at all wavelengths, see e.g., López et al. 2008).

Other HH objects show at least some degree of similarity between the two outflow lobes. Gyul’budagyan (1984) presents a discussion of the partially symmetric bipolar structure of the HH 1/2 outflow. The deviations from perfect symmetry in bipolar HH outflows were discussed by Bally & Reipurth (2001) and Woitas et al. (2002), who stud-

ied the asymmetries in the ejection density and velocity between the two outflow lobes.

Some IR bipolar outflows from young stellar objects (YSOs) show a surprising degree of “knot by knot” symmetry between the two outflow lobes. Examples of this are HH 212 (see, e.g., Smith, O’Connell, & Davis 2007; Cabrit et al. 2007) and HH 211 (e.g., Lee et al. 2010). In the well studied HH 34 and HH 111 optical outflows, it has been noted that good jet/counterjet knot symmetries are also present, particularly when one combines optical with IR observations (in which the highly obscured counterjets are detected). This was seen in HH 111 by Gredel & Reipurth (1994) and in HH 34 by García López et al. (2008).

Recent IR images obtained with the IRAC camera of *Spitzer* of HH 34 (Raga et al. 2011) and HH 111 (Noriega-Crespo et al. 2011) give us the possibility of directly measuring the positions of the knots (relative to the source) along the jet and counterjet in a single image, and to carry out a quantitative analysis of the degree of symmetry in the

¹Instituto de Ciencias Nucleares, Universidad Nacional Autónoma de México, Mexico.

²SPITZER Science Center, California Institute of Technology, CA, USA.

³Astronomisches Rechen-Institut Zentrum für Astronomie der Universität Heidelberg, Germany.

⁴Jet propulsion Laboratory, California Institute of Technology, CA, USA.

outflows. Such an analysis was not possible before because the HH 34 and 111 jets, counterjets, and outflow sources were not simultaneously detected in previous optical and/or near-IR images. Therefore, the *Spitzer* images open up a new possible analysis of HH outflows, because even though they have somewhat lower angular resolution than previous optical/IR images, they simultaneously show the source and the knots along the two outflow lobes.

Motivated by these new observations, in the present paper we develop a model of a jet with quasi-symmetric ejections of ballistic knots. The model predicts the behavior of the spatial offsets between jet/counterjet knot pairs as a function of increasing distance from the outflow source. The predicted dependence can then be compared with the knot positions measured in observed HH outflows in order to constrain the model parameters. A simpler model of this kind was described by Raga et al. (2011).

The paper is organized as follows. The ballistic, binary ejection model is described in § 2 (both the non-relativistic and the relativistic cases are considered). An application of the non-relativistic model to the observed positions of the jet/counterjet knots in HH 34 and 111 is described in § 3. Finally, the implications of the results are discussed in § 4.

2. A BALLISTIC, QUASI-SYMMETRIC BINARY EJECTION MODEL

2.1. Non-relativistic flows

Let us consider a non-relativistic, bipolar ejection with imperfect symmetry. In one direction (along the “jet”), a clump is ejected at a time τ with a velocity v_j (projected on the plane of the sky). In the opposite direction (along the “counterjet”), a clump is ejected at a time $\tau + \Delta\tau$, with a velocity $v_j - \Delta v$. If the parcels are ballistic, at a later time t they will be at distances x_j and x_{cj} (on the plane of the sky, along the jet and the counterjet, respectively) given by:

$$x_j = (t - \tau)v_j; \quad x_{cj} = (t - \tau - \Delta\tau)(v_j - \Delta v). \quad (1)$$

From this equation, one obtains that the offset $\Delta x = x_j - x_{cj}$ (between the positions of the jet and counterjet knots) grows with distance from the source, following

$$\Delta x = x_j - x_{cj} = \Delta\tau v_j + \frac{\Delta v}{v_j} x_j, \quad (2)$$

where we have neglected the term $\Delta\tau \Delta v$ (which involves the product of the two perturbations).

Now, let us assume that we have an ensemble of knot pairs, with $\Delta\tau$ and Δv values uniformly distributed in intervals $[\tau_0 - \Delta\tau_0, \tau_0 + \Delta\tau_0]$ and $[v_0 - \Delta v_0, v_0 + \Delta v_0]$, respectively. In other words, we allow for an intrinsic asymmetry in the ejection velocity Δv and in the time-delay $\Delta\tau$ between the jet/counterjet ejections.

The ensemble average of equation (2) is:

$$\begin{aligned} \langle \Delta x \rangle &= \int_{v_0 - \Delta v_0}^{v_0 + \Delta v_0} \int_{\tau_0 - \Delta\tau_0}^{\tau_0 + \Delta\tau_0} \Delta x \frac{d\Delta\tau d\Delta v}{4\Delta\tau_0 \Delta v_0} \\ &= \tau_0 v_j + \left(\frac{v_0}{v_j} \right) x_j. \end{aligned} \quad (3)$$

Therefore, the ensemble average of Δx as a function of x_j (where x_j is the distance to the successive knots measured along the jet) is a straight line with intercept a_1 and slope b_1 such that:

$$a_1 = \tau_0 v_j; \quad b_1 = \frac{v_0}{v_j}. \quad (4)$$

We should note that if we have an error of magnitude Δx_s in the estimated position of the source, we will obtain $a_1 = \tau_0 v_j \pm \Delta x_s$.

Also of interest is the quadratic average:

$$\begin{aligned} \langle (\Delta x)^2 \rangle &= \int_{v_0 - \Delta v_0}^{v_0 + \Delta v_0} \int_{\tau_0 - \Delta\tau_0}^{\tau_0 + \Delta\tau_0} \left[(\Delta\tau)^2 v_j^2 + \left(\frac{\Delta v x_j}{v_j} \right)^2 \right. \\ &\quad \left. + 2\Delta\tau \Delta v x_j \right] \frac{d\Delta\tau d\Delta v}{4\Delta\tau_0 \Delta v_0} \\ &= v_j^2 \left(\tau_0^2 + \frac{\Delta\tau_0^2}{3} \right) + \left(\frac{x_j}{v_j} \right)^2 \left(v_0^2 + \frac{\Delta v_0^2}{3} \right) + \tau_0 v_0 x_j. \end{aligned} \quad (5)$$

Therefore, the ensemble average of $(\Delta x)^2$ has a quadratic, $\langle (\Delta x)^2 \rangle = a_2 + b_2 x_j + c_2 x_j^2$ dependence with:

$$a_2 = v_j^2 \left(\tau_0^2 + \frac{\Delta\tau_0^2}{3} \right); \quad c_2 = \left(\frac{v_0}{v_j} \right)^2 + \frac{1}{3} \left(\frac{\Delta v_0}{v_j} \right)^2, \quad (6)$$

and with $b_2 = a_1 b_1$ given by the results of the fit to the $\langle \Delta x \rangle$ vs. x_j dependence (see equations 4 and 5).

To summarize, if one observes an outflow in which pairs of jet/counterjet knots can be identified, one has to make fits to the Δx vs. x_j and $(\Delta x)^2$ vs. x_j dependencies (where $\Delta x = x_j - x_{cj}$, the observed positional asymmetry between the jet/counterjet knot pairs). If one has an independent estimate of the spatial velocity v_j of the knots, the coefficients of the fits (see equations 4 and 6) directly give us the mean and half width of the ejection time (τ_0 and $\Delta\tau_0$) and velocity (v_0 and Δv_0) distributions.

2.2. Relativistic flows

Let us now consider the problem of quasi-symmetric, binary ejections at relativistic velocities. In § 2.1 (in which we considered a non-relativistic flow), we did not introduce the effect of projection onto the plane of the sky because the distances from the source and the jet velocity have the same plane-of-the-sky projection (and therefore, one can work with the projected distances and velocities).

In the case of a relativistic binary ejection, the clump ejected along the jet at a time τ with an intrinsic velocity v_j will be at a time t at a projected distance (from the source):

$$x_j = \frac{(t - \tau)v_j \cos \phi}{1 - v_j \sin(\phi/c)}, \quad (7)$$

where ϕ is the angle (towards the observer) between the jet axis and the plane of the sky, and c is the speed of light.

The clump ejected along the counterjet at a time $t + \Delta\tau$ with a velocity $v_j - \Delta v$ will be at a time t at a projected distance:

$$x_{cj} = \frac{(t - \tau - \Delta\tau)(v_j - \Delta v) \cos \phi}{1 + (v_j - \Delta v) \sin(\phi/c)}. \quad (8)$$

Combining equations (7-8) and expanding in a Taylor series up to first order in $\Delta\tau$ and Δv we obtain:

$$\begin{aligned} \Delta x = x_j - x_{cj} &= \frac{\Delta\tau v_j \cos \phi}{1 + v_j \sin(\phi/c)} \\ &+ \left[\frac{2v_j \sin(\phi/c)}{(1 + v_j \sin(\phi/c))} + \frac{(1 - v_j \sin(\phi/c))(\Delta v/v_j)}{(1 + v_j \sin(\phi/c))^2} \right] x_j. \end{aligned} \quad (9)$$

Carrying out the ensemble averages described in § 2.1, we then derive:

$$\langle \Delta x \rangle = A_1 + B_1 x_j; \quad \langle (\Delta x)^2 \rangle = A_2 + B_2 x_j + C_2 x_j^2, \quad (10)$$

with

$$\begin{aligned} A_1 &= \tau_0 v_j A, & B_1 &= B + C \frac{v_0}{v_j}, \\ A_2 &= A^2 \left(\tau_0^2 + \frac{\Delta\tau_0^2}{3} \right) v_j^2, & B_2 &= 2A(Bv_j + Cv_0)\tau_0, \\ C_2 &= \frac{C^2}{v_j^2} \left(v_0^2 + \frac{\Delta v_0^2}{3} \right) + B^2 + 2BC \frac{v_0}{v_j}, \end{aligned} \quad (11)$$

where A , B and C are the dimensionless functions

$$A = \frac{\cos \phi}{1 + v_j \sin(\phi/c)}, \quad B = \frac{2v_j \sin(\phi/c)}{(1 + v_j \sin(\phi/c))},$$

$$C = \frac{1 - v_j \sin(\phi/c)}{(1 + v_j \sin(\phi/c))^2}. \quad (12)$$

A , B and C are functions of order unity (except when $1 + v_j \sin(\phi/c) \ll 1$) for relativistic jets, with $v_j \sim c$. For $v_j \ll c$, they have limits $A = C = 1$ and $B = 0$. Inserting these values in equation (11) it is clear that we recover the non-relativistic equations (3–5) (considering that the velocities used in equation 11 correspond to the full spatial motion and not the projection on the plane of the sky considered in equations 3–5).

3. AN APPLICATION OF THE MODEL TO TWO HH JETS

3.1. Results of the model fit

We now apply the non-relativistic ballistic ejection model described in § 2.1 to two HH jets: HH 34 and HH 111. We first calculate least squares fits of the jet/counterjet knot offsets $\Delta x = x_j - x_{cj}$ and of $(\Delta x)^2$ as a function of distance x_j from the source. We then use the coefficients from the fits (together with an estimate of the knot velocities v_j) to constrain the ejection time ($\tau_0 \pm \Delta\tau_0$) and ejection velocity ($v_0 \pm \Delta v_0$) distributions resulting in the observed jet/counterjet asymmetries.

Given the fact that the distances and velocities along the jet/counterjet have identical projections onto the plane of the sky, we carry out the fitting procedure using the angular distances and proper motion velocities measured for the knot pairs. To obtain physical values from the angular distances and velocities, we assume a distance of 417 pc to HH 34 and 111 (see Menten et al. 2007).

3.2. The observations

The observations of HH 34 and HH 111 were downloaded from the *Spitzer* Heritage Archive⁵. They are part of our original General Observer (GO) program 3315 (PI Noriega-Crespo) obtained with the infrared camera IRAC (Fazio et al. 2004) and the infrared photometer MIPS (Rieke et al. 2004) in March 28, 2005. The high quality of the archival images (Post Basic Calibrated Data or Post-BCD; S18.7 products) was enough for our purposes and no further processing was required. The HH 34 and HH 111 observations with IRAC were taken in its four channels (1, 2, 3, 4) = (3.6, 4.5, 5.8 & 8.0 μm) and with a total integration time per pixel of 360 sec, using 30 sec High Dynamic Range (HDR) exposures. The final images are sampled with 0.6'' per pixel,

⁵<http://sha.ipac.caltech.edu/applications/Spitzer/SHA>.

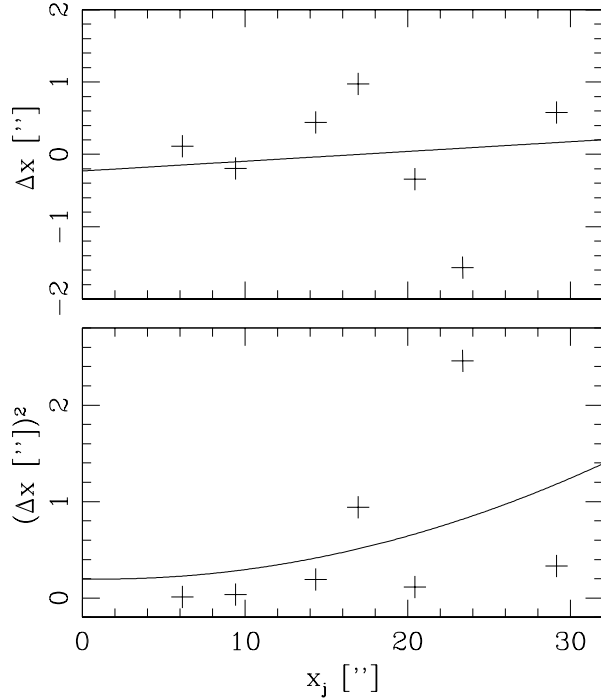


Fig. 1. Model fit to the HH 34 jet/counterjet knot pairs. We take the positions of the knots within $30''$ from the outflow source (from Raga et al. 2011) and plot $\Delta x = x_j - x_{c_j}$ (the jet/counterjet knot position offset, top graph) and $(\Delta x)^2$ (bottom graph) as a function of x_j . The straight line in the top graph and the curve in the bottom graph show the model fits, which result in the parameters given in Table 1.

nearly one third of the standard $\sim 2''$ IRAC angular resolution.

As described in Raga et al. (2011) and Noriega-Crespo et al. (2011), given the collisional excitation characteristics of young stellar outflows like HH 34 and 111, the emission in the IRAC bandpasses is likely to be dominated by the pure rotational H_2 lines (e.g., Noriega-Crespo et al. 2004a,b; Looney, Tobin & Kwon 2007; Tobin et al. 2007; Ybarra & Lada 2009; De Buizer & Vacca 2010). Finally, in the HH 111 image we carried out astrometry of several field stars in order to correctly locate the position of the VLA 1 source (the source of the HH 111 outflow, see, e.g., Rodríguez et al. 2008).

3.3. The HH 34 knots

For the HH 34 outflow, we consider the 7 quasi-symmetric knot pairs detected in the *Spitzer* image of Raga et al. (2011). These knots lie at angular distances $< 30''$ from the source, and have a clear correspondence between the jet and the counterjet.

TABLE 1
FITS TO THE HH 34/111 KNOTS

	HH 34	HH 111
a_1	$(-0.23 \pm 0.72)''$	$(2.19 \pm 0.85)''$
b_1	0.024 ± 0.039	0.027 ± 0.011
a_2	$(0.20 \pm 0.48)''^2$	$(8.5 \pm 4.1)''^2$
c_2	$(1.26 \pm 1.10) \times 10^{-3}$	$(0.93 \pm 0.42) \times 10^{-3}$
v_j	150 km s^{-1}	240 km s^{-1}
τ_0	$(-3.0 \pm 9.5) \text{ yr}$	$(18.1 \pm 7.0) \text{ yr}$
v_0	$(2.0 \pm 5.9) \text{ km s}^{-1}$	$(6.5 \pm 2.6) \text{ km s}^{-1}$
$\Delta\tau_0$	$(8.8 \pm 17.4) \text{ yr}$	$(27.7 \pm 20.5) \text{ yr}$
Δv_0	$(9.0 \pm 5.6) \text{ km s}^{-1}$	$(10.9 \pm 5.8) \text{ km s}^{-1}$

The results of the least squares fits to the Δx vs. x_j and $(\Delta x)^2$ vs. x_j dependencies are shown in Figure 1. The coefficients of the (linear Δx vs. x_j and quadratic $(\Delta x)^2$ vs. x_j) fits, together with the errors estimated through the fitting procedure, are given in Table 1.

Proper motion measurements (see, e.g., Reipurth et al. 2002) indicate that the knots close to the source of the HH 34 system have plane of the sky velocities $v_j \approx 150 \text{ km s}^{-1}$. Using this velocity and the parameters derived from the fits, from equations (4–6) we obtain the mean values of the widths of the ejection time (τ_0 and Δv_0) and of the ejection velocity (v_0 and Δv_0) distributions. The resulting values (together with their uncertainties) are given in Table 1.

3.4. The HH 111 knots

Noriega-Crespo et al. (2011) present a *Spitzer* image of the HH 111 system. This system does not show such a clearly symmetric structure as the HH 4 outflow. This fact is illustrated in Figure 2.

From the observed jet and counterjet structures, we choose a set of 5 well defined knot pairs which appear to have clear jet/counterjet correspondences (see Figure 2). We then use these 5 knot pairs to obtain the Δx vs. x_j and $(\Delta x)^2$ vs. x_j dependencies. The fits to these dependencies are shown in Figure 3, and the resulting coefficients are given in Table 1.

From the values of the coefficients from the fits and a $v_j \approx 240 \text{ km s}^{-1}$ plane of the sky velocity (see, e.g., Hartigan et al. 2001), we obtain the parameters of the ejection time and velocity distributions (τ_0 , $\Delta\tau_0$ and v_0 , Δv_0 , respectively). These parameters are given in Table 1.

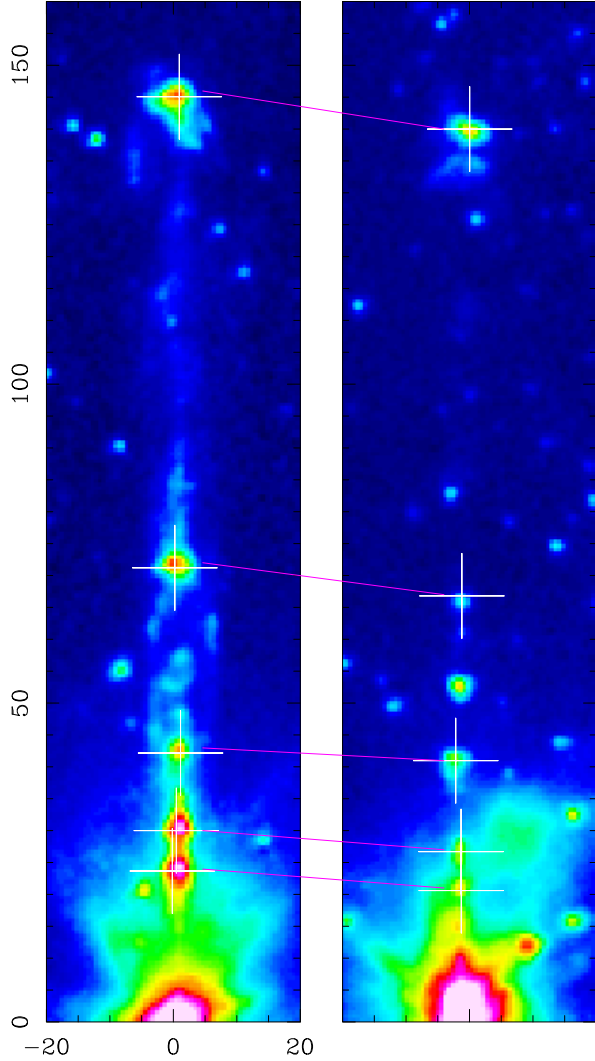


Fig. 2. The HH 111 *Spitzer* IRAC I2 band image of Noriega-Crespo et al. (2011), displayed in two frames. The left frame shows the E lobe, and the right frame the W lobe of HH 111. In both cases, the outflow axis has been rotated so that the outflow is parallel to the ordinate. In both frames, the source is placed at the origin of the reference system. The arrows indicate the chosen jet/counterjet knot pairs, and the crosses show the positions determined from parabolic fits to the emission peaks of the knots. The axes are labeled in arcseconds. The color figure can be viewed online.

3.5. Discussion

From Table 1, we see that the ejection asymmetries deduced for the HH 34 and HH 111 outflows differ from each other in a significant way. If we look at the average values τ_0 and v_0 of the ejection time and velocity offsets (respectively), we find that:

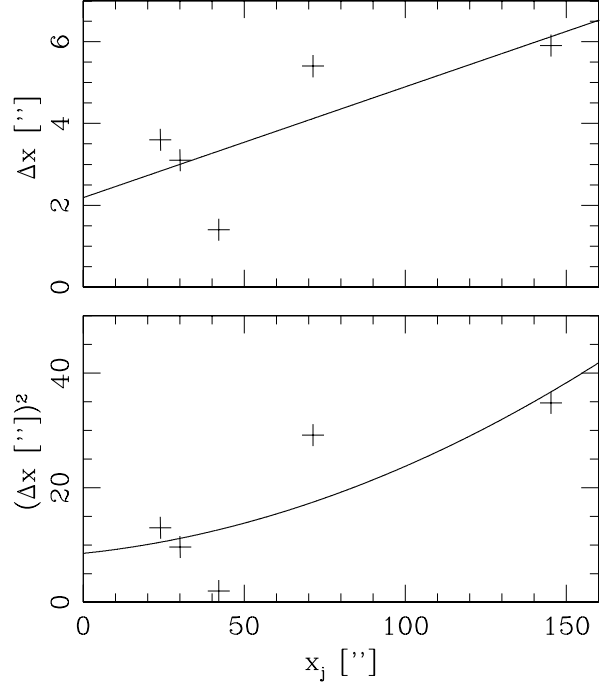


Fig. 3. Model fit to the HH 111 jet/counterjet knot pairs. We take the positions of the knot pairs shown in Figure 2 and plot Δx (top graph) and $(\Delta x)^2$ (bottom graph) as a function of x_j . The straight line in the top graph and the curve in the bottom graph show the model fits, which result in the parameters given in Table 1.

- the knot structure of HH 34 implies ejection asymmetries with average time [$\tau_0 = (-3.0 \pm 9.5)$ yr] and velocity [$v_0 = (2.0 \pm 5.9)$ km s⁻¹] offsets which are not significantly different from zero,
- the positions of the knots of HH 111 imply non-zero average time [$\tau_0 = (18.2 \pm 7.1)$ yr] and velocity [$v_0 = (6.5 \pm 2.6)$ km s⁻¹] offsets.

As it is explained after equation (4), the non-zero value of τ_0 determined for HH 111 could be due to an error in the estimated position for the outflow source. For HH 111 the required offset would be $\Delta x_s = \tau_0 v_j \approx 2''.2$. Given the fact that we have located the source of HH 111 with an accuracy of better than one pixel ($\approx 0''.6$), it is clear that the average time offset that we find for the HH 111 ejections is not dominated by a possible error in the position of the outflow source. The $v_0 = (6.5 \pm 2.6)$ km s⁻¹ average velocity offset also is undoubtedly a real effect.

For the widths of the ejection time and velocity offset distributions (see Table 1) we obtain that:

- HH 34 has a time offset distribution with a $\Delta\tau_0 = (8.9 \pm 17.3)$ yr width, which is not significantly different from zero. The velocity offset distribution has a $\Delta v_0 = (9.0 \pm 5.6)$ km s⁻¹ width,
- HH 111 implies a time offset distribution with $\Delta\tau_0 = (27.7 \pm 20.5)$ yr and $\Delta v_0 = (10.9 \pm 5.8)$ km s⁻¹.

4. CONCLUSIONS

We have presented a simple, ballistic binary ejection model for interpreting the observed knot structures of quasi-symmetric bipolar outflows. In this model it is assumed that knots are ejected with small time ($\Delta\tau$) and velocity (Δv) offsets, which result in a slightly asymmetric propagation as the knots move away from the source. It is also assumed that these offsets have uniform distributions with mean values τ_0 and v_0 and half-widths $\Delta\tau_0$ and Δv_0 (for the time and velocity offsets, respectively). Under these assumptions, we show that the values of τ_0 , v_0 , $\Delta\tau_0$ and Δv_0 can be recovered from observations of the spatial jet/counterjet knot offsets $\Delta x = x_j - x_{cj}$ for a system of identifiable knot pairs.

We then apply this method to recent *Spitzer* observations of the HH 34 (Raga et al. 2011) and HH 111 (Noriega-Crespo et al. 2011) jet/counterjet systems. We find that the knots of the HH 34 outflow imply binary ejections with basically zero systematic jet/counterjet ejection times or velocities. The dispersion of the ejection times also lies below the errors due to small number statistics. However, the observed spatial distribution of the jet/counterjet knot offsets does imply a non-zero value for the width of the ejection velocity distribution [$\Delta v_0 = (9.0 \pm 5.6)$ km s⁻¹, see Table 1].

As noted by Raga et al. (2011), the good time coordination of the binary ejections of HH 34 imply that the triggering of the ejection events occurs in a compact region. Even though we are not able to obtain a well constrained value for the time-offsets between the jet and counterjet knots, we can take as an estimate either the value of τ_0 or of $\Delta\tau_0$ (both ~ 5 yr, see Table 1). If we assume a (sound or Alfvén) wave propagation velocity $v_s \sim 3$ km s⁻¹ for the jet formation region, this coordination timescale then implies a size $d \sim 3$ AU.

A clearly different result is obtained for HH 111. The jet/counterjet knot pairs of this system imply a clear bias towards one side, with the clumps in the W lobe being ejected on average a time $\tau_0 = (18.2 \pm 7.1)$ yr later and $v_0 = (6.5 \pm 2.6)$ km s⁻¹ slower than the corresponding knots in the E lobe. The observa-

tions also imply non-zero widths for the ejection time and velocity distributions ($\Delta\tau_0 = (27.7 \pm 20.5)$ yr and $\Delta v_0 = (10.9 \pm 5.8)$ km s⁻¹, respectively, see Table 1).

For HH 111 we then conclude that an intrinsically asymmetric ejection is taking place, with one side producing faster and earlier ejections than the other. Such an effect is seen at least in one other YSO outflow: Curiel et al. (2006) present high resolution radio continuum maps at many epochs of the Cepheus A HW2 outflow, and they find that the knots are ejected ~ 2 yr earlier in one of the two lobes. It appears that in HH 111 we are seeing a similar effect, but with a time-delay that is larger by one order of magnitude.

The systematic velocity offset ($v_0 \approx 6.5$ km s⁻¹, see Table 1) of the HH 111 jet/counterjet knots could actually be the result of a non-ballistic behavior of the motion. For example, if the knots along one of the outflow lobes were interacting directly with a denser medium, this interaction could lead to a lower velocity knot propagation velocity. However, as the knots are traveling into the wake of previous ejection episodes, such a direct knot/environment interaction seems unlikely. Also, the different velocities could in principle be the result of different orientations of the lobes with respect to the plane of the sky. However, the very small deviations from a straight path on the plane of the sky observed in HH 111 (see Noriega-Crespo et al. 2011) do not favor this scenario.

The asymmetries in the ejections of the HH 34 and 111 knots in principle provide constraints on the jet production model. However, in many cases it is not yet possible to apply these constraints because the present models for the production of outflows from young stars are either stationary (e.g., Salmeron, Königl, & Wardle 2011) or do not appear to incorporate the mechanism(s) that produce the knots observed along HH jets (e.g., Ramsey & Clarke 2011; Stute et al. 2010; Yamada et al. 2009). A recent analysis of models producing asymmetric ejections (as the result of the presence of a time-independent magnetospheric magnetic field with both a dipole and a quadrupole component) is given by Lovelace et al. (2010), who for some parameters obtain outflows that “flip-flop” with a period of ~ 30 days. Given the fact that this predicted timescale is a factor of 10–100 times too small for explaining the asymmetries observed for the HH 34 and 111 knots, it is clear that if one is to rescue the ideas of Lovelace et al. (2010) it will be necessary to introduce other elements. A possibility would be the presence of a time-variability in the magnetospheric magnetic field, as explored by De Colle, García, &

Murphy (2008). The magnetospheric magnetic field could have time-dependencies on timescales similar to the solar cycle (i.e., with periods ~ 20 yr).

From the observational point of view, significant progress will be possible through the analysis of other bipolar HH jets. Such studies should include both objects with good jet/counterjet symmetries (such as HH 211, see, e.g., Lee et al. 2010) and objects with evident asymmetries (such as HH 228, see Wang & Henning 2009).

Finally, in § 2.2 we have described a model for relativistic, quasi-symmetric binary ejections. An application of this model to observations of relativistic jets is left for a future paper.

This work was supported by the Conacyt grants 61547, 101356 and 101975.

REFERENCES

- Bally, J., & Reipurth, B. 2001, *ApJ*, 546, 299
- Cabrit, S., Codella, C., Gueth, F., Nisini, B., Gusdorf, A., Dougados, C., & Bacciotti, F. 2007, *A&A*, 468, L29
- Curiel, S., Raga, A. C., Raymond, J. C., Noriega-Crespo, A., & Cantó, J. 1997, *AJ*, 114, 2736
- Curiel, S., et al. 2006, *ApJ*, 638, 878
- De Buizer, J. M., & Vacca, W. D. 2010, *AJ*, 140, 196
- De Colle, F., Gracia, J., & Murphy, G. 2008, *ApJ*, 688, 1137
- Fazio, G., et al. 2004, *ApJS*, 154, 10
- García López, R., Nisini, B., Giannini, T., Eisloffel, J., Bacciotti, F., & Podio, L. 2008, *A&A*, 487, 1019
- Gredel, R., & Reipurth, B. 1994, *A&A*, 289, L19
- Gyul'budagyan, A. L. 1984, *Astrophysics*, 20, 75
- Hartigan, P., Morse, J. A., Reipurth, B., Heathcote, S., & Bally, J. 2001, *ApJ*, 559, L157
- Lee, C.-F., Hasegawa, T. I., Hirano, N., Palau, A., Shang, H., Ho, P. T. P., & Zhang, Q. 2010, *ApJ*, 713, 731
- Looney, L. W., Tobin, J. J., & Kwon, W. 2007, *ApJ*, 670, L131
- López, R., García-Lorenzo, B., Sánchez, S. F., Gómez, G., Estalella, R., & Riera, A. 2008, *MNRAS*, 391, 1107
- Lovelace, R. V. E., Romanova, M. M., Ustyugova, G. V., & Koldoba, A. V. 2010, *MNRAS*, 408, 2083
- Menten, K. M., Reid, M. J., Forbrich, J., & Brunthaler, A. 2007, *A&A*, 474, 515
- Noriega-Crespo, A., et al. 2004a, *ApJS*, 154, 352
- Noriega-Crespo, A., et al. 2004b, *ApJS*, 154, 402
- Raga, A. C., Noriega-Crespo, A., Lora, V., Stapelfeldt, K. R., & Carey, S. J. 2011, *ApJ*, 730, L17
- Ramsey, J. P., & Clarke, D. A. 2011, *ApJ*, 728, L11
- Reipurth, B., Heathcote, S., Morse, J., Hartigan, P., & Bally, J. 2002, *AJ*, 123, 362
- Rieke, G. H., et al. 2004, *ApJS*, 154, 25
- Rodríguez, L. F., Torrelles, J. M., Anglada, G., & Reipurth, B. 2008, *AJ*, 136, 1852
- Salmeron, R., Königl, A., & Wardle, M. 2011, *MNRAS*, 412, 1162
- Smith, M. D., O'Connell, B., & Davis, C. J. 2007, *A&A*, 466, 565
- Stute, M., Gracia, J., Tsinganos, K., & Vlahakis, N. 2010, *A&A*, 516, A6
- Tobin, J. J., Looney, L. W., Mundy, L. G., Kwon, W., & Hamidouche, M. 2007, *ApJ*, 659, 1404
- Wang, H., & Henning, T. 2009, *AJ*, 138, 1072
- Woitas, J., Ray, T. P., Bacciotti, F., Davis, C. J., & Eisloffel, J. 2002, *ApJ*, 580, 336
- Yamada, M., Machida, M. N., Inutsuka, S., & Tomisaka, K. 2009, *ApJ*, 703, 1141
- Ybarra, J. E., & Lada, E. A. 2009, *ApJ*, 695, 120

S. J. Carey and A. Noriega-Crespo: Spitzer Science Center, California Institute of Technology, Pasadena, CA 91125, USA (carey, alberto@ipac.caltech.edu).

V. Lora: Astronomisches Rechen-Institut Zentrum für Astronomie der Universität Heidelberg, Mönchhofstr. 12-14 69120 Heidelberg, Germany (vlora@ari.uni-heidelberg.de).

A. C. Raga and J. C. Rodríguez-Ramírez: Instituto de Ciencias Nucleares, Universidad Nacional Autónoma de México, Apdo. Postal 70-543, 04510 D.F., Mexico (raga, juan.rodriguez@nucleares.unam.mx).

K. R. Stapelfeldt: Jet propulsion Laboratory, California Institute of Technology, MS 183-900, 4800 Oak Grove Drive, Pasadena, CA 91109, USA (krs@exoplanet.jpl.nasa.gov).